BNL-213711-2020-JAAM

Lanthanide-Binding Tags for 3D X-ray Imaging of Proteins in Cells at Nanoscale Resolution

T. W. Victor,

To be published in "JOURNAL OF THE AMERICAN CHEMICAL SOCIETY"

February 2020

Photon Sciences

Brookhaven National Laboratory

U.S. Department of Energy

USDOE Office of Science (SC), Basic Energy Sciences (BES) (SC-22)

Notice: This manuscript has been authored by employees of Brookhaven Science Associates, LLC under Contract No. DE-SC0012704 with the U.S. Department of Energy. The publisher by accepting the manuscript for publication acknowledges that the United States Government retains a non-exclusive, paid-up, irrevocable, world-wide license to publish or reproduce the published form of this manuscript, or allow others to do so, for United States Government purposes.

DISCLAIMER

This report was prepared as an account of work sponsored by an agency of the United States Government. Neither the United States Government nor any agency thereof, nor any of their employees, nor any of their contractors, subcontractors, or their employees, makes any warranty, express or implied, or assumes any legal liability or responsibility for the accuracy, completeness, or any third party's use or the results of such use of any information, apparatus, product, or process disclosed, or represents that its use would not infringe privately owned rights. Reference herein to any specific commercial product, process, or service by trade name, trademark, manufacturer, or otherwise, does not necessarily constitute or imply its endorsement, recommendation, or favoring by the United States Government or any agency thereof or its contractors or subcontractors. The views and opinions of authors expressed herein do not necessarily state or reflect those of the United States Government or any agency thereof.

Lanthanide-Binding Tags for 3D X-Ray Imaging of Proteins in Cells at Nanoscale Resolution

Tiffany W. Victor[1,2] Katherine H. O'Toole,[3] Lindsey M. Easthon,[3] Mingyuan Ge,[1] Randy J. Smith,[1] Xiaojing Huang,[1] Hanfei Yan,[1] Yong S. Chu,[1] Si Chen,[4] Doga Gursoy,[4,5] Martina Ralle,[6] Barbara Imperiali,[7] Karen N. Allen,[3] and Lisa M. Miller[1,2]*

[1] National Synchrotron Light Source II, Brookhaven National Laboratory, Upton, NY, 11973

[2] Department of Chemistry, Stony Brook University, Stony Brook, NY, 11794

[3] Department of Chemistry, Boston University, Boston, MA, 02215

[4] Advanced Photon Source, Argonne National Laboratory, Argonne, IL, 60439

[5] Department of Electrical Engineering and Computer Science, Northwestern University, Evanston, IL, 60298

[6] Department of Molecular and Medical Genetics, Oregon Health Science University, Portland, OR 97239

[7] Department of Biology, Massachusetts Institute of Technology, Cambridge, MA, 02139

Supporting Information Placeholder

ABSTRACT: We report the application of lanthanide-binding tags (LBTs) for two- and three-dimensional X-ray imaging of individual proteins in cells with a sub-15 nm beam. The method combines encoded LBTs, which are tags of minimal size (ca 15-20 amino acids) affording high-affinity lanthanide ion binding, and X-ray Fluorescence Microscopy (XFM). This approach enables visualization of LBT-tagged proteins while simultaneously measuring the elemental distribution in cells at a spatial resolution necessary for visualizing cell membranes and eukaryotic subcellular organelles.

X-ray Fluorescence Microscopy (XFM) is a powerful method for imaging the trace-element concentration, distribution, and speciation in cells and tissues. Even though the technique has been around for more than 30 years, only recently have advances in X-ray sources, optics, and detectors enabled two- and three-dimensional imaging at the nanoscale with attogram detection sensitivity.[1-4] A few recent examples include the observation of "zinc sparks" in oocyte fertilization,[5] copper binding to amyloid plaques in Alzheimer's disease,[6] manganese accumulation within nanovesicles of the Golgi apparatus in Parkinson's disease,[7] new approaches for neuroprotection with chemotherapy treatment,[8] and heme detoxification by the malaria parasite.[9]

Despite the recent advancements in focusing optics[10] and faster fluorescence detectors,[11-12] the spatial resolution of XFM has been limited to a few hundred nanometers in 2D and typically the micron scale in 3D making it difficult to image subcellular organelles and individual proteins. Here, we address this challenge by taking advantage of the development of new multilayer Laue X-ray lenses (MLLs) for imaging in 2D and 3D with a sub-15 nm beam.[13]

Additionally, there are very few X-ray sensitive tags for co-localizing individual proteins of interest with the trace-element distribution in subcellular structures. [14-15] Today, fluorescence microscopy is a ubiquitous method for imaging individual proteins within the context of a living cell, where fluorescent labeling with proteins and small molecules via methods such as bioorthogonal conjugation and genetically encoded fusion tags have provided target-specific visualization.[16-17] But there remain major opportunities for the development of new methods and tags to enhance spatial resolution with minimal interruption of native structures and interactions.

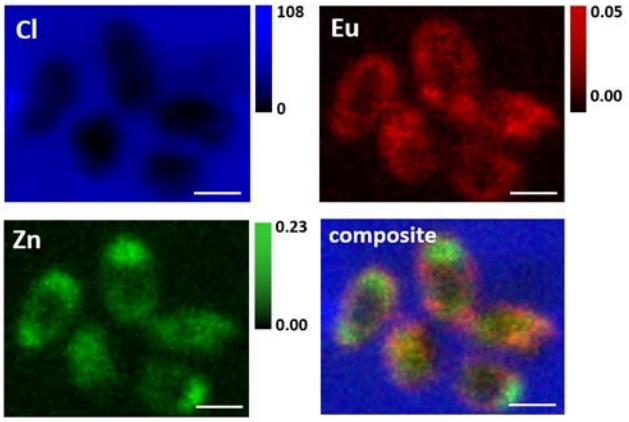

Figure 1. XFM images showing the distribution of Cl, Eu, Zn, and the overlay of Eu (red), Zn (green) and Cl (blue) in *E. coli* cells expressing OmpA-LBT and incubated with 5 µm Eu. Images were collected with zone plate optics and a 85 nm beam size. Scale bar is 2 microns and concentration units are µg/cm^2.

In this study, we build upon the concept of using encoded fusion tags as a method for visualizing specific proteins in cells by introducing X-ray sensitive tags that improve the image resolution beyond the diffraction limit of visible light. Lanthanide-binding tags (LBTs) are short peptides (15-20 amino acids) comprised almost entirely of a nanomolar-affinity lanthanide-binding domain.[18-20] When complexed to a lanthanide ion, the LBT in a fusion protein has previously been used for investigations involving photoluminescence,[21] NMR spectroscopy,[22-24] MRI,[25] and X-ray crystallography.[26-27]

We have adapted the use of LBTs for XFM, with the goal of imaging individual target proteins at a spatial resolution approaching 10 nm within intact cells, while simultaneously co-localizing the trace-element distribution and concentration. As lanthanides are rare in living organisms, the use of LBTs provides a protein-specific tag for visualizing proteins with XFM without competing signals from endogenous metal ions. The LBTs can easily be incorporated into the target protein sequence, and their small size minimizes any deleterious effects on target protein expression, function, or transport within the cell. The high affinity of the LBTs for lanthanides means that experiments can be performed at a low lanthanide concentration to mitigate toxic effects. The dissociation constants for Eu^{3+} and Er^{3+} with a single LBT are 62±4 nM and 78±6 nM, respectively. [28]

For LBTs to be useful for nanoscale cellular imaging, they must be detectable at low concentrations, where the background signal (e.g. non-specific binding) is minimized. First, we demonstrate the use of trivalent Eu- and Er-LBTs to image a membrane protein, Outer Membrane Protein A (OmpA), located on the surface of Escherichia coli *(E. coli*) (**Figure 1**). Amongst membrane proteins, OmpA is abundant at a copy number of 100,000 per cell.[29]

Here, *E. coli* cells were embedded in small NaCl crystals (1-20 μm), which we have found to maintain the three-dimensional shape of the cells.[4] In addition, the cells provide a negative contrast in the Cl XRF image, making them easy to locate. **Figure 1** shows a cluster of five *E. coli* cells embedded in NaCl crystals wherein OmpA was tagged with the LBT (YIDTNNDWIEGDEL) into an outward-facing loop and the cells were exposed to 5 μM $EuCl_3$. The XFM images of the Cl, Eu, and Zn distributions are shown, along with the 3-color composite image. The outline of the cells can be visualized in the Cl image, where they appear as dark regions among the NaCl crystals.

The Eu XFM image shows that Eu is mostly concentrated at the outer surface of the cells. As Eu is not endogenous to the cell, it is only expected to be associated with the LBT which is bound to the extracellular loop of OmpA. Hence the XFM image is consistent with a membrane-bound Eu-LBT.

XFM can simultaneously detect multiple trace elements in the cell, so other elements were also examined. The Zn image shows an inhomogeneous distribution in some cells where the Zn concentration is localized at the poles. In bacteria, divalent zinc is strongly associated with the ribosomes, which are typically located at the polar-end caps of cells[30-33] and has been observed with XFM previously.[4]

We also examined the ability to visualize proteins tagged with LBTs in the cytosol (**Figure 2**). In this case, a double LBT (dLBT; YIDTNNDGWIEGDELYIDTNNDGWIEGDELLA) was fused to the N-terminus of ubiquitin (Ubi-dLBT) and heterologously expressed in *E. coli* with $ErCl_3$ added at the time of induction. Ubiquitin and ubiquitin-like proteins are abundant in cells and act as protein modifiers that regulate proteosomal degradation.[34-36] For example in HEK293 cells, the ubiquitin concentration is ~85 μM in both free and conjugated species.[37]

For visualizing intracellular proteins, the detection sensitivity is also dependent upon the transport of the lanthanide into the cells. Although the entry of lanthanide ions is not yet fully understood, studies suggest that lanthanides are transported into the cytosol via the sodium-calcium exchanger and calcium-ion pumps using electrochemical gradients.[38-39] They may also be transported via phagocytosis, endocytosis, and pinocytosis.[40] Inductively Coupled Plasma Mass Spectrometry (ICP-MS) performed on the OmpA-LBT cells as a function of Eu concentration showed that the lanthanide reduced both the potassium and calcium concentrations in the cells, supporting the literature reports of ion-channel transport (**Figure S1**).

Figure 2 shows the optical and XFM images of a cluster of seven *E. coli* cells expressing Er-loaded Ubi-dLBT. The Ca image shows that this ion is homogeneously distributed in all cells. A similar uniform distribution was seen for Er, which is consistent with the fact that ubiquitin is expressed throughout the cell. [41] However, although Er was uniformly distributed, it was only visualized in one dividing cell, which can clearly be seen in the 3-color composite image, indicating that the lanthanide uptake efficiency and/or tag expression need to be further optimized for future studies. In cells not expressing Ubi-dLBT, there was no discrete emission signal in the presence of Er, suggesting that the lanthanide ions are concentrated in the cell by mass action via LBT binding.

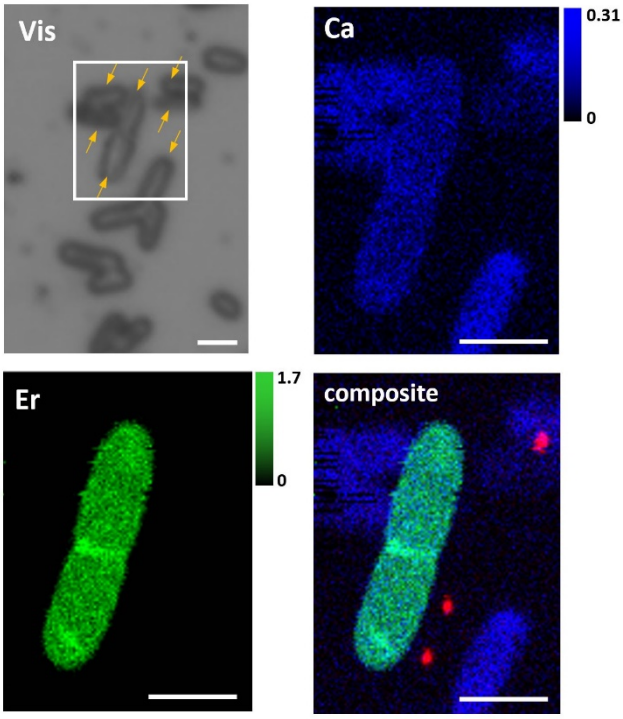

Figure 2. Visible light image shows *E. coli* cells with Ubi-dLBT incubated with 1 mM Er. XFM images show the distribution of Ca, Er, and the overlay of Ca and Er in the *E. coli* cells. Au nanoballs (in red) are 100 nm in diameter and were added as fiducial markers for tomography reconstruction. Images were collected with zone plate optics and an 85 nm beam size. Scale bar is 2 microns and concentration units are $\mu g/cm^2$. In the visible image, each yellow arrow indicates an *E.coli* cell.

X-ray fluorescence spectra from Ubi-dLBT-encoded cells exposed to 1 mM $EuCl_3$, revealed distinct Eu X-ray fluorescence (**Figure S2**). Without expression of the tag, i.e. uninduced Ubi-dLBT, the Eu fluorescence peaks are absent. Similarly, for OmpA, distinct X-ray fluorescence peaks for Eu were seen at 5.85 keV ($L_{\alpha 1}$) and 6.46 keV ($L_{\beta 1}$) (**Figure S2**). However, in cells that were exposed to Eu in the absence of the OmpA-LBT construct, X-ray fluorescence peaks from Eu were absent.

The design of LBTs is such that the binding site can accommodate different lanthanides, all with nanomolar affinity.[42-43] Since the fluorescence spectra are fitted to extract the concentration of the element present in the cells, it is beneficial to choose a lanthanide that minimizes overlaps of fluorescence emission lines with the trace element(s) of interest (**Table S1**). For example, the L_α and L_β peaks of Eu are found at 5.85 keV and 6.46 keV, respectively. In

this spectral range, the Mn K_α and Fe K_α peaks fall at 5.90 keV and 6.40 keV, respectively, and can overlap with the Eu signal. This overlap can be reduced by using Er-LBT, where the L_α and L_β peaks fall at 6.95 and 7.81 keV respectively. However, although there would be no overlap with the Mn K_α, there would be an overlap with the Fe K_β and Cu K_α.(**Figure S2**). Hence, the appropriate lanthanide should be selected based on the trace element(s) of interest in the study.

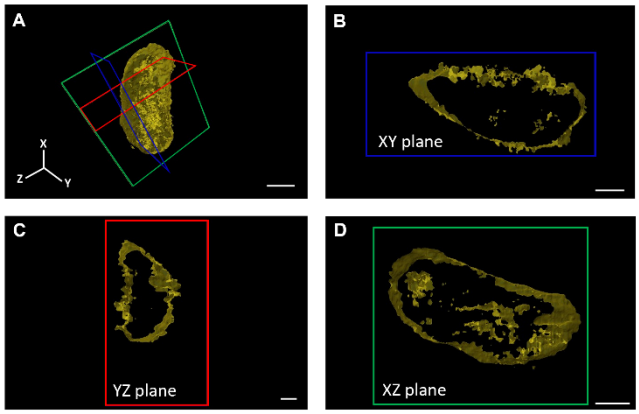

Figure 3. **(A)** Isosurface plot showing the Erbium X-ray nanotomogram of a single *E. coli* cell expressing OmpA-LBT and incubated with Er. Virtual slices through the cell are seen in the XY, YZ and XZ planes in **(B)**, **(C),** and **(D),** respectively. During the tomography scan, the cell was rotated along the XZ axis. The thickness of the illustrated sections in B-D are approximately 40 nm, 115 nm, and 138 nm in the XY, YZ and XZ planes, respectively. Scale bar is 500 nm.

Due to the long penetration depth of X-rays, XFM with LBT-fusion proteins can also be used to visualize targeted proteins in cells in three dimensions. Tomographic imaging is particularly important for localizing proteins in subcellular structures and organelles at the nanoscale, e.g. visualizing membrane proteins. Tomographic imaging was performed on a single *E. coli* cell expressing OmpA-LBT and exposed to $ErCl_3$. During the tomography scan, the cell was rotated along the XZ (green) axis plane and imaged with a 15 nm X-ray beam. Er isosurface images **(Figure 3)** were calculated from the normalized X-ray fluorescence intensity reconstruction (**Figure S3**). Using power spectral analysis, a spatial resolution of 36 nm was calculated from the 3D Er tomography reconstruction **(Figure S4**).

Supplemental Video 1 shows the three-dimensional distribution of zinc and erbium in the cell. The zinc distribution is consistent with the findings observed in **Figure 1**, i.e. the zinc is distributed throughout the cell with the highest concentrations at the polar end caps. For the Er distribution, the tomogram shows a "shell" of Er on the surface, with a smaller amount of Er interior to the cell. These findings can also be seen in **Figure 3**. For the XY and YZ planes (**Figures 3B** and **3C**, respectively), the Er appears primarily located on the outer surface of the cell. However, for the XZ plane in **Figure 3D**, there is also evidence of some Er within the cell.

The primary role for OmpA in *E. coli* is to stabilize the outer membrane via the beta-barrel structure.[44-46] The high copy number of OmpA has made it a target for incorporation of other fusion tags in the exterior loops including GFP[47] and FLAG and C-Myc epitope tags,[48] both of which have demonstrated the shell-like structure at lower resolution. Dynamics studies have shown that OmpA is immobile in the outer membrane, with no long-range lateral diffusion.[49]

In addition to its structural role in the outer membrane, OmpA has also been shown to act as a porin.[50] Its porin activity is slow and produces non-specific diffusion channels for various small solutes with low permeability.[51] As such, it is often a target for antibiotic resistance.[52-54] Due to its non-specific transport properties, OmpA may be a route for lanthanides to transit the outer membrane to the periplasm, gaining access to transporters, thereby facilitating entry and providing an explanation for the presence of a small amount of erbium inside the cell.

In summary, lanthanide-binding tags (LBTs) can be used for 2D and 3D nanoscale imaging with X-rays. LBTs are short peptides comprising a nanomolar-affinity lanthanide-binding domain. The high affinity of LBTs for lanthanides allows experiments to be performed at low concentrations, thereby mitigating toxic effects. The LBTs can be easily incorporated into target protein sequences, and their small size minimizes deleterious effects on target protein expression, function, or transport within the cell. Here we demonstrate successful X-ray imaging of two LBT-protein conjugates, a membrane protein (OmpA) and a soluble protein (ubiquitin) with nanoscale spatial resolution. As the conjugation of LBTs and proteins follow standard molecular biology protocols, we propose that XFM with LBTs could become a widespread tool for 3D imaging of protein distribution and localization within cells with a high spatial resolution while simultaneously obtaining trace element distribution. Moreover, the long penetration depth of X-rays enables nanoscale visualization of the internal structure of cells in 3D, allowing for the extension of the method to tissues.

ASSOCIATED CONTENT

Supporting Information

The Supporting Information is available free of charge on the ACS Publications website.

Detailed experimental methods, image analysis, tomographic reconstruction, and mass spectrometry data (PDF) and 3D tomographic video (MPG).

AUTHOR INFORMATION

Corresponding Author

*lmiller@bnl.gov

Notes

The authors declare no competing financial interests.

ACKNOWLEDGMENT

This work was supported by the United States Department of Energy, Office of Biological and Environmental Research, as part of the "Environment Sensing and Response" Scientific Focus Area of the BER Genomic Science Program. TWV was partially supported by the National Institutes of Health T32 Grant 5T32GM092714 and a Director's Postdoctoral Fellowship at NSLS-II. BI and KNA were supported by NSF MCB- 1615252 and MCB-1614608, respectively. This research used resources of beamline 3-ID (HXN) at NSLS-II, a U.S. Department of Energy (DOE) Office of Science User Facilities operated for the DOE Office of Science by Brookhaven National Laboratory under Contract No. DE-SC0012704. This research used resources of the BNP beamline at APS, a U.S. Department of Energy (DOE) Office of Science User Facilities operated for the DOE Office of Science by Argonne National Laboratory under Contract No. DE-AC02-06CH11357.

REFERENCES

1. Paunesku, T.; Vogt, S.; Maser, J.; Lai, B.; Woloschak, G., X-ray fluorescence microprobe imaging in biology and medicine. *J Cell Biochem* **2006,** *99* (6), 1489-502.
2. de Jonge, M. D.; Vogt, S., Hard X-ray fluorescence tomography--an emerging tool for structural visualization. *Curr Opin Struct Biol* **2010,** *20* (5), 606-14.
3. Kashiv, Y.; Austin, J. R., 2nd; Lai, B.; Rose, V.; Vogt, S.; El-Muayed, M., Imaging trace element distributions in single organelles and subcellular features. *Sci Rep* **2016,** *6*, 21437.
4. Victor, T. W.; Easthon, L. M.; Ge, M.; O'Toole, K. H.; Smith, R. J.; Huang, X.; Yan, H.; Allen, K. N.; Chu, Y. S.; Miller, L. M., X-ray Fluorescence Nanotomography of Single Bacteria with a Sub-15 nm Beam. *Sci Rep* **2018,** *8* (1), 13415.
5. Que, E. L.; Bleher, R.; Duncan, F. E.; Kong, B. Y.; Gleber, S. C.; Vogt, S.; Chen, S.; Garwin, S. A.; Bayer, A. R.; Dravid, V. P.; Woodruff, T. K.; O'Halloran, T. V., Quantitative mapping of zinc fluxes in the mammalian egg reveals the origin of fertilization-induced zinc sparks. *Nat Chem* **2015,** *7* (2), 130-9.
6. Bourassa, M. W.; Leskovjan, A. C.; Tappero, R. V.; Farquhar, E. R.; Colton, C. A.; Van Nostrand, W. E.; Miller, L. M., Elevated copper in the amyloid plaques and iron in the cortex are observed in mouse models of Alzheimer's disease that exhibit neurodegeneration. *Biomed Spectrosc Imaging* **2013,** *2* (2), 129-139.
7. Carmona, A.; Zogzas, C. E.; Roudeau, S.; Porcaro, F.; Garrevoet, J.; Spiers, K. M.; Salome, M.; Cloetens, P.; Mukhopadhyay, S.; Ortega, R., SLC30A10 Mutation Involved in Parkinsonism Results in Manganese Accumulation within Nanovesicles of the Golgi Apparatus. *ACS Chem Neurosci* **2019,** *10* (1), 599-609.
8. Popovic, J.; Klajn, A.; Paunesku, T.; Ma, Q.; Chen, S.; Lai, B.; Stevanovic, M.; Woloschak, G. E., Neuroprotective Role of Selected Antioxidant Agents in Preventing Cisplatin-Induced Damage of Human Neurons In Vitro. *Cell Mol Neurobiol* **2019,** *39* (5), 619-636.
9. Kapishnikov, S.; Grolimund, D.; Schneider, G.; Pereiro, E.; McNally, J. G.; Als-Nielsen, J.; Leiserowitz, L., Unraveling heme detoxification in the malaria parasite by in situ correlative X-ray fluorescence microscopy and soft X-ray tomography. *Sci Rep* **2017,** *7* (1), 7610.
10. Mimura, H., Advances in Hard X-ray Focusing Optics. *Synchrotron Radiation News* **2016,** *29* (4), 2-2.
11. Somogyi, A.; Mocuta, C., Possibilities and Challenges of Scanning Hard X-ray Spectro-microscopy Techniques in Material Sciences. *AIMS Materials Science* **2015,** *2* (2), 122-162.
12. Kopittke, P. M.; Punshon, T.; Paterson, D. J.; Tappero, R. V.; Wang, P.; Blamey, F. P. C.; van der Ent, A.; Lombi, E., Synchrotron-Based X-Ray Fluorescence Microscopy as a Technique for Imaging of Elements in Plants. *Plant Physiology* **2018,** *178* (2), 507-523.
13. Yan, H.; Bouet, N.; Zhou, J.; Huang, X.; Nazaretski, E.; Xu, W.; Cocco, A. P.; Chiu, W. K. S.; Brinkman, K. S.; Chu, Y. S., Multimodal hard x-ray imaging with resolution approaching 10 nm for studies in material science. *Nano Futures* **2018,** *2* (1), 011001.
14. Hostachy, S.; Masuda, M.; Miki, T.; Hamachi, I.; Sagan, S.; Lequin, O.; Medjoubi, K.; Somogyi, A.; Delsuc, N.; Policar, C., Graftable SCoMPIs enable the labeling and X-ray fluorescence imaging of proteins. *Chem Sci* **2018,** *9* (19), 4483-4487.
15. Vogt, S.; Ralle, M., Opportunities in multidimensional trace metal imaging: taking copper-associated disease research to the next level. *Anal Bioanal Chem* **2013,** *405* (6), 1809-1820.
16. Baddeley, D.; Bewersdorf, J., Biological Insight from Super-Resolution Microscopy: What We Can Learn from Localization-Based Images. *Annual Review of Biochemistry* **2018,** *87* (1), 965-989.
17. Sahl, S. J.; Hell, S. W.; Jakobs, S., Fluorescence nanoscopy in cell biology. *Nat Rev Mol Cell Biol* **2017,** *18* (11), 685-701.
18. Franz, K. J.; Nitz, M.; Imperiali, B., Lanthanide-binding tags as versatile protein coexpression probes. *Chembiochem* **2003,** *4* (4), 265-71.
19. Barthelmes, K.; Reynolds, A. M.; Peisach, E.; Jonker, H. R.; DeNunzio, N. J.; Allen, K. N.; Imperiali, B.; Schwalbe, H., Engineering encodable lanthanide-binding tags into loop regions of proteins. *J Am Chem Soc* **2011,** *133* (4), 808-19.
20. Allen, K. N.; Imperiali, B., Lanthanide-tagged proteins--an illuminating partnership. *Current opinion in chemical biology* **2010,** *14* (2), 247-54.
21. Sculimbrene, B. R.; Imperiali, B., Lanthanide-binding tags as luminescent probes for studying protein interactions. *J Am Chem Soc* **2006,** *128* (22), 7346-52.
22. Martin, L. J.; Hahnke, M. J.; Nitz, M.; Wohnert, J.; Silvaggi, N. R.; Allen, K. N.; Schwalbe, H.; Imperiali, B., Double-lanthanide-binding tags: design, photophysical properties, and NMR applications. *J Am Chem Soc* **2007,** *129* (22), 7106-13.
23. Su, X. C.; McAndrew, K.; Huber, T.; Otting, G., Lanthanide-binding peptides for NMR measurements of residual dipolar couplings and paramagnetic effects from multiple angles. *J Am Chem Soc* **2008,** *130* (5), 1681-7.
24. Morgan, A. J.; Prasciolu, M.; Andrejczuk, A.; Krzywinski, J.; Meents, A.; Pennicard, D.; Graafsma, H.; Barty, A.; Bean, R. J.; Barthelmess, M.; Oberthuer, D.; Yefanov, O.; Aquila, A.; Chapman, H. N.; Bajt, S., High numerical aperture multilayer Laue lenses. *Scientific Reports* **2015,** *5* (1).
25. Daughtry, K. D.; Martin, L. J.; Sarraju, A.; Imperiali, B.; Allen, K. N., Tailoring encodable lanthanide-binding tags as MRI contrast agents. *Chembiochem* **2012,** *13* (17), 2567-74.
26. Silvaggi, N. R.; Martin, L. J.; Schwalbe, H.; Imperiali, B.; Allen, K. N., Double-lanthanide-binding tags for macromolecular crystallographic structure determination. *J Am Chem Soc* **2007,** *129* (22), 7114-20.
27. Martin, L. J. Development of lanthanide-binding tags (LBTs) as powerful and versatile peptides for use in studies of proteins and protein interactions. Thesis (Ph.D.), Massachusetts Institute of Technology, Dept. of Chemistry, Cambridge, MA, 2008.
28. Nitz, M.; Sherawat, M.; Franz, K. J.; Peisach, E.; Allen, K. N.; Imperiali, B., Structural origin of the high affinity of a chemically evolved lanthanide-binding peptide. *Angew Chem Int Edit* **2004,** *43* (28), 3682-3685.
29. Parent, K. N.; Erb, M. L.; Cardone, G.; Nguyen, K.; Gilcrease, E. B.; Porcek, N. B.; Pogliano, J.; Baker, T. S.; Casjens, S. R., OmpA and OmpC are critical host factors for bacteriophage Sf6 entry in Shigella. *Molecular microbiology* **2014,** *92* (1), 47-60.
30. Bakshi, S.; Siryaporn, A.; Goulian, M.; Weisshaar, J. C., Superresolution Imaging of Ribosomes and RNA Polymerase in Live Escherichia coli Cells. *Molecular Microbiology* **2012,** *85* (1), 21-38.
31. Dillon, S. C.; Dorman, C. J., Bacterial nucleoid-associated proteins, nucleoid structure and gene expression. *Nat Rev Micro* **2010,** *8* (3), 185-195.
32. Takahashi, H.; Oshima, T.; Hobman, J. L.; Doherty, N.; Clayton, S. R.; Iqbal, M.; Hill, P. J.; Tobe, T.; Ogasawara, N.; Kanaya, S.; Stekel, D. J., The dynamic balance of import and export of zinc in Escherichia coli suggests a heterogeneous population response to stress. *Journal of The Royal Society Interface* **2015,** *12* (106).
33. Blindauer, C. A., Advances in the molecular understanding of biological zinc transport. *Chemical Communications* **2015,** *51* (22), 4544-4563.
34. Ohtake, F.; Tsuchiya, H.; Saeki, Y.; Tanaka, K., K63 ubiquitylation triggers proteasomal degradation by seeding branched ubiquitin chains. *Proceedings of the National Academy of Sciences* **2018,** *115* (7), E1401-E1408.
35. Pearce, M. J.; Mintseris, J.; Ferreyra, J.; Gygi, S. P.; Darwin, K. H., Ubiquitin-Like Protein Involved in the Proteasome Pathway of Mycobacterium tuberculosis. *Science* **2008,** *322* (5904), 1104-1107.
36. Yau, R.; Rape, M., The increasing complexity of the ubiquitin code. *Nature Cell Biology* **2016,** *18* (6), 579-586.
37. Kaiser, S. E.; Riley, B. E.; Shaler, T. A.; Trevino, R. S.; Becker, C. H.; Schulman, H.; Kopito, R. R., Protein standard absolute quantification (PSAQ) method for the measurement of cellular ubiquitin pools. *Nature methods* **2011,** *8* (8), 691-696.
38. Szasz, I.; Sarkadi, B.; Schubert, A.; Gardos, G., Effects of lanthanum on calcium-dependent phenomena in human red cells. *Biochim Biophys Acta* **1978,** *512* (2), 331-40.
39. Powis, D. A.; Clark, C. L.; O'Brien, K. J., Lanthanum can be transported by the sodium-calcium exchange pathway and directly triggers catecholamine release from bovine chromaffin cells. *Cell Calcium* **1994,** *16* (5), 377-390.
40. Cheng, Y.; Huo, Q.; Lu, J.; Li, R.; Wang, K., The transport kinetics of lanthanide species in a single erythrocyte probed by confocal laser scanning microscopy. *Journal of biological inorganic chemistry : JBIC : a publication of the Society of Biological Inorganic Chemistry* **1999,** *4* (4), 447-56.
41. Lecker, S. H.; Goldberg, A. L.; Mitch, W. E., Protein Degradation by the Ubiquitin–Proteasome Pathway in Normal and Disease States.

Journal of the American Society of Nephrology **2006,** *17* (7), 1807-1819.
42. Reynolds, A. M.; Sculimbrene, B. R.; Imperiali, B., Lanthanide-Binding Tags with Unnatural Amino Acids: Sensitizing Tb3+ and Eu3+ Luminescence at Longer Wavelengths. *Bioconjugate Chemistry* **2008,** *19* (3), 588-591.
43. Peacock, A. F. A., Chapter Twenty-Four - De Novo Designed Imaging Agents Based on Lanthanide Peptides Complexes. In *Methods in Enzymology*, Pecoraro, V. L., Ed. Academic Press: 2016; Vol. 580, pp 557-580.
44. Wang, Y., The function of OmpA in Escherichia coli. *Biochem Biophys Res Commun* **2002,** *292* (2), 396-401.
45. Abe, T.; Murakami, Y.; Nagano, K.; Hasegawa, Y.; Moriguchi, K.; Ohno, N.; Shimozato, K.; Yoshimura, F., OmpA-like protein influences cell shape and adhesive activity of Tannerella forsythia. *Mol Oral Microbiol* **2011,** *26* (6), 374-87.
46. Rojas, E. R.; Billings, G.; Odermatt, P. D.; Auer, G. K.; Zhu, L.; Miguel, A.; Chang, F.; Weibel, D. B.; Theriot, J. A.; Huang, K. C., The outer membrane is an essential load-bearing element in Gram-negative bacteria. *Nature* **2018,** *559* (7715), 617-621.
47. Shi, H.; Wen Su, W., Display of green fluorescent protein on Escherichia coli cell surface. *Enzyme Microb Technol* **2001,** *28* (1), 25-34.
48. Verhoeven, G. S.; Alexeeva, S.; Dogterom, M.; den Blaauwen, T., Differential bacterial surface display of peptides by the transmembrane domain of OmpA. *PLoS One* **2009,** *4* (8), e6739.
49. Verhoeven, G. S.; Dogterom, M.; den Blaauwen, T., Absence of long-range diffusion of OmpA in E. coli is not caused by its peptidoglycan binding domain. *BMC Microbiol* **2013,** *13*, 66.
50. Confer, A. W.; Ayalew, S., The OmpA family of proteins: roles in bacterial pathogenesis and immunity. *Vet Microbiol* **2013,** *163* (3-4), 207-22.
51. MacIntyre, S.; Henning, U., The role of the mature part of secretory proteins in translocation across the plasma membrane and in regulation of their synthesis in Escherichia coli. *Biochimie* **1990,** *72* (2-3), 157-67.
52. Sugawara, E.; Nikaido, H., OmpA is the principal nonspecific slow porin of Acinetobacter baumannii. *J Bacteriol* **2012,** *194* (15), 4089-96.
53. Iyer, R.; Moussa, S. H.; Durand-Reville, T. F.; Tommasi, R.; Miller, A., Acinetobacter baumannii OmpA Is a Selective Antibiotic Permeant Porin. *ACS Infect Dis* **2018,** *4* (3), 373-381.
54. Choi, U.; Lee, C. R., Distinct Roles of Outer Membrane Porins in Antibiotic Resistance and Membrane Integrity in Escherichia coli. *Front Microbiol* **2019,** *10*, 953.
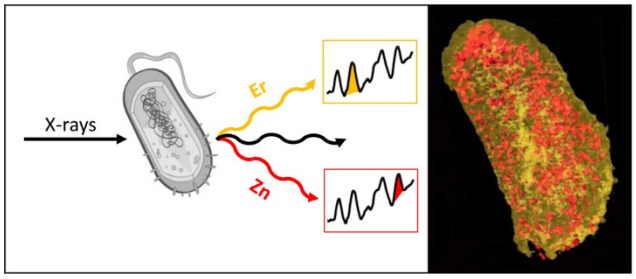
Insert Table of Contents artwork here